Line field optical coherence tomography: in vivo diagnosis of basal cell carcinoma subtypes compared with histopathology

C. Ruini, Sandra Schuh, C. Gust, B. Kendziora, L. Frommherz, L. E. French, D. Hartmann, Julia Welzel, E. Sattler

Angaben zur Veröffentlichung / Publication details:

Ruini, C., Sandra Schuh, C. Gust, B. Kendziora, L. Frommherz, L. E. French, D. Hartmann, Julia Welzel, and E. Sattler. 2021. "Line field optical coherence tomography: in vivo diagnosis of basal cell carcinoma subtypes compared with histopathology." *Clinical and Experimental Dermatology* 46 (8): 1471–81. https://doi.org/10.1111/ced.14762.

Original article

CED
Clinical and Experimental Dermatology

Line-field optical coherence tomography: *in vivo* diagnosis of basal cell carcinoma subtypes compared with histopathology

C. Ruini,[1,2] S. Schuh,[3] C. Gust,[1] B. Kendziora,[1] L. Frommherz,[1] L. E. French,[1,4] D. Hartmann,[1] J. Welzel[3] and E. Sattler[1]

[1]*Department of Dermatology and Allergy, University Hospital, LMU, Munich, Germany;* [2]*PhD School in Clinical and Experimental Medicine, University of Modena and Reggio Emilia, Italy;* [3]*Department of Dermatology and Allergy, University Hospital, Augsburg, Germany; and* [4]*Dr Phillip Frost Department of Dermatology and Cutaneous Surgery, University of Miami, Miller School of Medicine, Miami, FL, USA*

doi:10.1111/ced.14762

Summary

Background. Basal cell carcinoma (BCC) is the most common skin cancer in the general population. Treatments vary from Mohs surgery to topical therapy, depending on the subtype. Dermoscopy, reflectance confocal microscopy (RCM) and optical coherence tomography (OCT) have gained a foothold in daily clinical practice to optimize diagnosis and subtype-oriented treatment. The new technique of line-field confocal OCT (LC-OCT) allows imaging at high resolution and depth, but its use has not yet been investigated in larger studies.

Aim. To evaluate the main LC-OCT criteria for the diagnosis and subtyping of BCC compared with histopathology, OCT and RCM.

Methods. In total, 52 histopathologically confirmed BCCs were evaluated for imaging criteria. Their frequency, predictive values and ROC curves were calculated. A multinominal regression with stepwise variables selection to distinguish BCC subtypes was performed.

Results. Nodular BCCs were mainly characterized by atypical keratinocytes, altered dermoepidermal junction (DEJ), tumour nests in the dermis, dark clefting, prominent vascularization and white hyper-reflective stroma. Superficial BCCs showed a thickening of the epidermis due to a series of tumour lobules with clear connection to the DEJ (string of pearls pattern). Infiltrative BCCs were characterized by elongated hyporeflective tumour strands, surrounded by bright collagen (shoal of fish pattern). The overall BCC subtype agreement between LC-OCT and conventional histology was 90.4% (95% CI 79.0–96.8).

Conclusion. LC-OCT allows noninvasive, real-time identification of BCCs and their subtypes in vertical, horizontal and three-dimension mode compared with histology, RCM and OCT. Further larger studies are needed to better explore the clinical applications of this promising device.

Introduction

Basal cell carcinoma (BCC) is the most commonly occurring type of skin cancer in the general population. Because advanced tumours can be locally destructive and disfiguring, early detection and treatment are essential to limit destructive surgical procedures and their complications, economic burden and patient discomfort.[1] In a real-life setting, clinical and dermoscopic examination helps with identification of

Correspondence: Dr Cristel Ruini, Department of Dermatology and Allergy, University Hospital, LMU Munich, Frauenlobstr. 9-11, Munich, 80337, Germany
E-mail: cristel.ruini@med.uni-muenchen.de

Conflict of interest: the authors declare that they have no conflicts of interest.

JW and ES contributed equally to this work and should be considered joint senior authors.

Accepted for publication 25 May 2021

lesions suspicious for BCC. Patients with such lesions may then proceed to diagnostic or therapeutic procedures. Histology is accepted as the gold-standard assessment tool for BCC subtyping, which then directly guides the treatment offered to patients.[1] As biopsies are expensive and time-consuming and carry additional risks, noninvasive diagnostic methods have gained a foothold in daily clinical practice.[2] Among these, reflectance confocal microscopy (RCM), conventional and high-definition optical coherence tomography (OCT) and multiphoton microscopy have been used to increase diagnostic accuracy and to allow noninvasive BCC subtyping.[3–9] The main imaging criteria for diagnosing BCCs have been described in numerous studies as having diagnostic sensitivity and specificity values > 90%.[9–11]

Nevertheless, such technologies have minor disadvantages. Although RCM has a high resolution (horizontal < 1.25 μm, vertical < 5.0 μm), its penetration depth of 200–250 μm only reaches the superficial dermis. By contrast, OCT has a penetration depth of up to 1.5 mm, but its resolution is only about 7.5 μm (lateral) to 5 μm (axial).

The new technique of line-field confocal OCT (LC-OCT) allows the simultaneous display of horizontal and vertical images with both cellular resolution (axial 1.1 μm, lateral 1.3 μm) and a detection depth ($\sim$500 μm) that reaches to the mid-dermis. Healthy skin, various skin tumours and mite infestations have all been investigated by LC-OCT in pilot studies.[1–18] Moreover, a recently published study[18] described the main morphological criteria for BCC subtypes in LC-OCT. The aim of the current work was to evaluate the advantages and limitations of LC-OCT in the diagnosis of BCC and in the differentiation of BCC subtypes validated by histopathology in a clinical setting. A secondary aim was to compare a subgroup of LC-OCT BCC images with corresponding RCM and OCT images of the same lesion, focusing on diagnostic confidence.

Methods

The study protocol was reviewed and approved by the institutional review board of LMU Munich (approval no. 17-699) and written informed consent was obtained from all participants.

Study population

Patients were prospectively recruited and evaluated for the main imaging criteria in the context of a global study on pigmented and nonpigmented lesions examined with LC-OCT. We later included in the statistical analysis only previously untreated cases that had been completely excised after image review and confirmed as BCCs by subsequent histopathological examination and complete excision: 25 nodular (n)BCCs, 11 superficial (s)BCCs, 5 infiltrative (i)BCCs and 11 nodular–superficial (ns)BCCs. Four of the five iBCCs also included minor nodular components, but were clustered as infiltrative based on their predominant appearance. The nsBCCs had a homogeneous distribution of both components.

Images

Clinical, dermoscopic and LC-OCT images [horizontal, vertical, three-dimensional (3D) mode] were collected in all cases. Additionally and depending on patient consent. OCT images in horizontal (*en face*) view (6 × 6 mm in 31 cases: 13 nBCCs, 9 sBCCs, 2 iBCCs and 7 mBCCs) and RCM multiple Vivastacks (500 × 500 μm) and Vivablocks (5 × 5 mm) images (22 cases: 9 nBCCs, 4 sBCCs, 1 iBCC and 7 nsBCCs). In each case, the whole tumour area was scanned. Images were evaluated by four trained dermatologists (CR, SS, LF, ES) and agreement reached by consensus. Discordant cases were discussed with two dermatologists (DH, JW) who are experts in dermatopathology. Histopathological slides were analysed by the senior pathologist of each centre.

Imaging devices

The LC-OCT system (DAMAE Medical, Paris, France) is classified as a class 1 supercontinuum laser, and uses a central wavelength of 800 nm. Combining the principle of OCT interferometry with the spatial filtering of RCM, the device collects multiple A-scans parallel to the skin surface to a depth of $\sim$500 μm, while constantly adjusting its focus. It has three imaging modalities displayed as a grey scale: vertical or *en coupe*, horizontal or *en face* and 3D stack for a 3D reconstruction, with a vertical and horizontal field of view of 1.2 × 0.5 mm^2. Details have been described in previous studies.[14,17,19–21] Conventional OCT images were acquired with Vivosight (Michelson Diagnostics Ltd, Maidstone, Kent, UK), RCM images with Vivascope 1500 (Mavig GmbH, Munich, Germany) and clinical–dermoscopic images with Fotofinder (FotoFinder GmbH, Berlin, Germany) and Dermogenius 2 (Dermoscan GmbH, Regensberg, Germany).

Imaging features

The main diagnostic patterns were selected based on previous publications. The dermoscopic features are described in Table 1. For LC-OCT, a selection of criteria based on histological diagnostic features and previously described OCT and RCM terminology was developed (Table 1).[22–25] In addition, image quality and confidence with diagnosis and subtype were reported semiquantitatively (low < 50%, average 50–75%, high > 75%).

Statistical analysis

For descriptive statistics, mean ± SD were calculated for numerical variables, while absolute numbers with percentage values were used for nominal variables. To evaluate the diagnostic accuracy of LC-OCT in detecting different BCC subtypes, the sensitivity, specificity, positive predictive value (PPV), negative predictive value (NPV), and area under the curve of the receiver-operating characteristic curve were calculated. Dermatopathology was considered the gold standard. Multinomial regression with stepwise selection of variables was used to search for LC-OCT characteristics that would differentiate between BCC subtypes. Variables without explanatory value as measured by the Akaike information criterion were excluded by bidirectional elimination. All statistics were performed in *R* software (V3.6.0, 2; *R* Foundation for Statistical Computing, Vienna, Austria). $P < 0.05$ was considered statistically significant.

Results

Epidemiology

In total, 52 patients (35 men, 17 women, mean age 71 years) with Fitzpatrick skin phototypes I–III with

Table 1 Main line-field confocal optical coherence tomography in detecting different basal cell carcinoma subtypes evaluated in the study with their relative and absolute frequencies.

	BCC subtype									
	All		Nodular		Superficial		Infiltrative		Nodular–superficial	
Orientation	%	*n/N*	%	*n/N*	%	*n/N*	%	*n/N*	%	*n/N*
En coupe (vertical)										
Epidermis										
Hyperkeratosis	32.7	17/52	32.0	8/25	9.1	1/11	60.0	3/5	45.5	5/11
Thinning	46.2	24/52	44.0	11/25	36.4	4/11	40.0	2/5	63.6	7/11
Scales	26.9	14/52	24.0	6/25	27.3	3/11	40.0	2/5	27.3	3/11
Keratin plugs	5.8	3/52	8.0	2/25	0	0/11	0	0/5	9.1	1/11
Ulceration	21.2	11/52	16.0	4/25	18.2	2/11	20.0	1/5	36.4	4/11
Atypical keratinocytes	76.9	40/52	68.0	17/25	81.8	9/11	0	0/5	100.0	11/11
DEJ and dermis										
Alteration of the DEJ profile	98.1	51/52	96.0	24/25	100.0	11/11	100.0	5/5	100.0	11/11
Tumour nests/lobules	98.1	51/52	100.0	25/25	100.0	11/11	80.0	4/5	100.0	11/11
Clefting	96.2	50/52	100.0	25/25	90.9	10/11	80.0	4/5	100.0	11/11
Prominent vessels/neoangiogenesis	96.2	50/52	92.0	23/25	100.0	11/11	100.0	5/5	100.0	11/11
Bright structures	42.3	22/52	56.0	14/25	18.2	2/11	20.0	1/5	45.5	5/11
Shoal of fish pattern	13.5	7/52	4.0	1/25	0	0/11	100.0	5/5	9.1	1/11
String of pearls pattern	42.3	22/52	12.0	3/25	90.9	10/11	20.0	1/5	72.7	8/11
White hyper-reflective stroma	94.2	49/52	92.0	23/25	90.9	10/11	100.0	5/5	100.0	11/11
Black areas/cysts	19.2	10/52	12.0	3/25	18.2	2/11	40.0	2/5	27.3	3/11
Cell polarization	67.3	35/52	64.0	16/25	72.7	8/11	80.0	4/5	63.6	7/11
En face (horizontal)										
Atypical honeycomb	76.9	40/52	68.0	17/25	81.8	9/11	0	0/5	100.0	11/11
Clefting	53.8	28/52	60.0	15/25	45.5	5/11	40.0	2/5	54.5	6/11
Cord-like structures	11.5	6/52	8.0	2/25	36.4	4/11	0	0/5	0	0/11
Dark silhouettes	46.2	24/52	40.0	10/25	63.6	7/11	60.0	3/5	36.4	4/11
Tumour nests/lobules	65.5	33/52	72.0	18/25	36.4	4/11	60.0	3/5	72.7	8/11
Canalicular vessels	71.2	37/52	76.0	19/25	72.7	8/11	80.0	4/5	54.5	6/11
Collagen alterations	98.1	51/52	100.0	25/25	90.9	10/11	100.0	5/5	100.0	11/11

BCC, basal cell carcinoma; DEJ, dermoepidermal junction.

histologically confirmed BCCs were enrolled in the study. Most BCCs arose in the head and neck area (51.9%), followed by the trunk (34.6%) and limbs (13.5%).

Diagnostic confidence

Diagnostic confidence for BCC subtype (high, average and low, respectively) was 44.2%, 42,3% and 13.5% for dermoscopy, and 78.8%, 15.4% and 5.8% for LC-OCT. LC-OCT increased the examiners' diagnostic confidence by 36.5%. Diagnostic confidence (high and average, respectively) was 68% and 24% for OCT, and 44% and 31.5% for RCM was: high. LC-OCT image quality was high in 75% of cases and average in the remaining 25%.

Imaging features

The main dermoscopic features are shown in Table S1, and the main overall LC-OCT features of BCCs are shown in Table 1.

In vertical mode, nBCCs were mainly characterized by atypical keratinocytes in the epidermis above them (68%), an altered dermoepidermal junction (DEJ) profile as determined by connected or underlying tumour lobules (96%), tumour nests/lobules in the dermis (100%), dark clefting (100%), prominent vessels (92%) and white hyper-reflective stroma (92%). In horizontal mode, an atypical honeycomb pattern (68%), tumour nests/lobules (72%), dark silhouettes (40%) and collagen alterations (100%) were seen (Figs 1 and 2; Fig. S1, Video S1, Table 1).

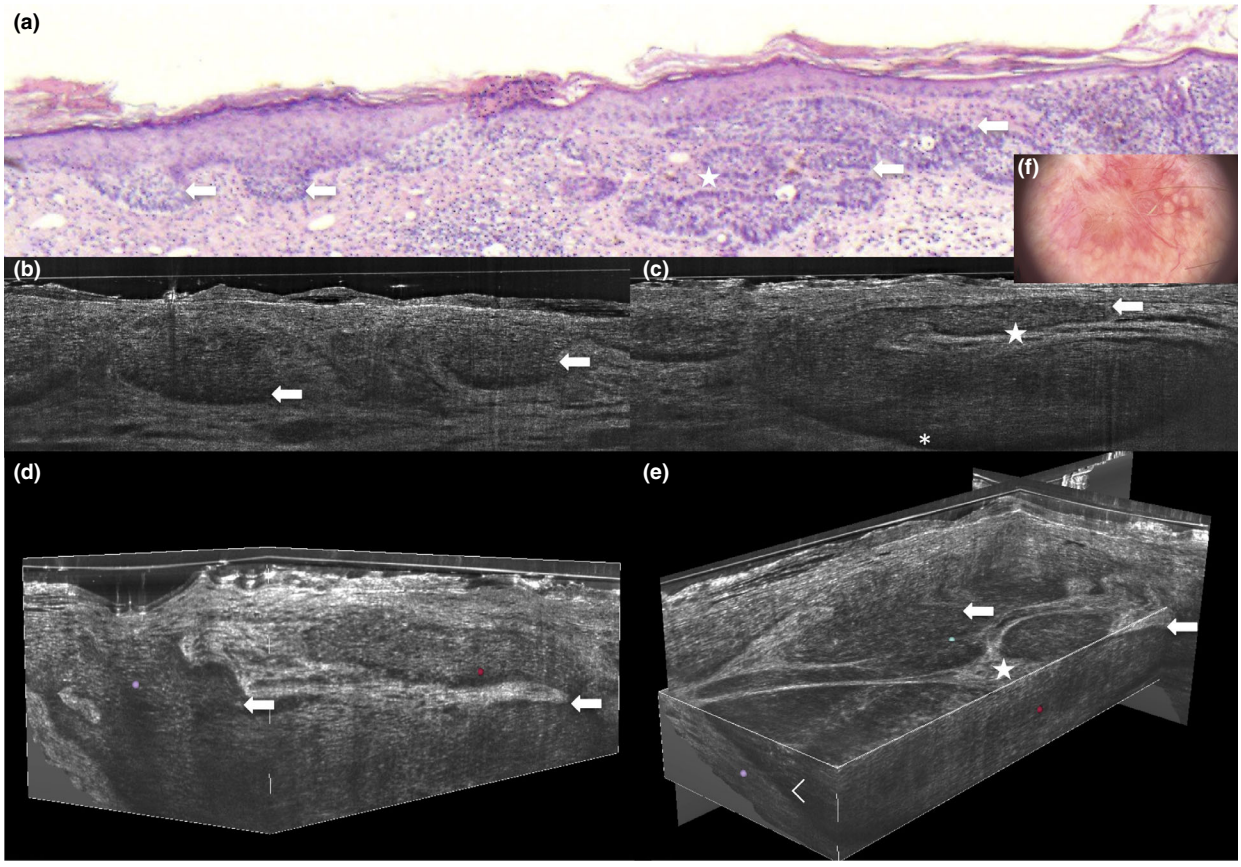

Figure 1 (a–f) Appearance of a nodular–superficial basal cell carcinoma of the face in a 60-year-old man as visualized by (a) conventional microscopy (haematoxylin and eosin, original magnification × 100), (b–e) line-field confocal optical coherence tomography in (b, c) vertical and (d, e) three-dimensional mode, and (f) dermoscopy (original magnification × 10). Note the hyporeflective ovoid structures arranged in a string of pearls pattern (arrow), together with the beginning of nodular components (arrow), which have lost their connection to the epidermis, separated by a discrete stromal reaction (star).

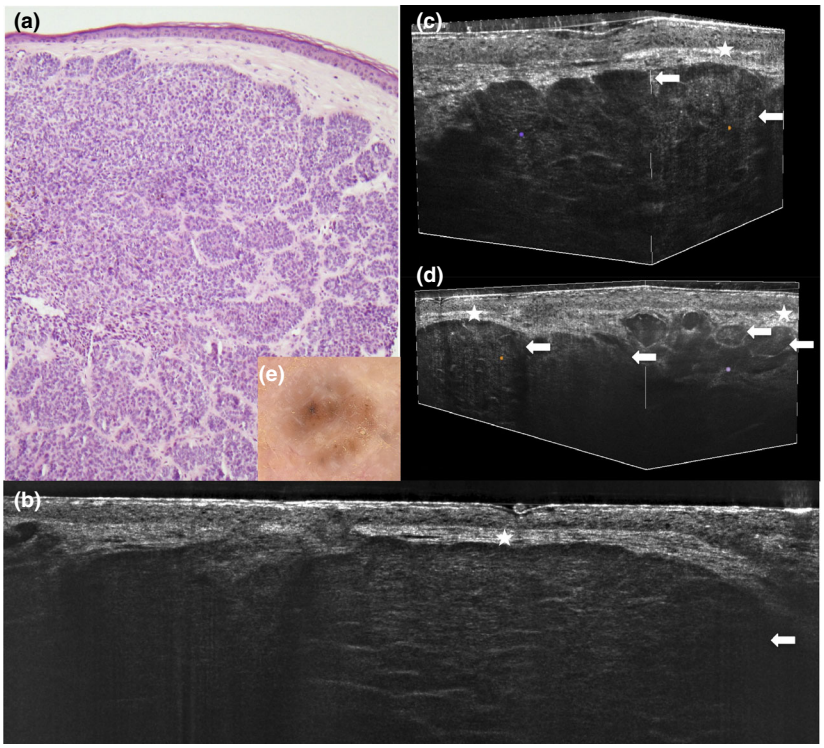

Figure 2 (a–e) Appearance of a nodular–micronodular basal cell carcinoma of the face in a 75-year-old woman, as visualized by (a) conventional microscopy (haematoxylin and eosin, original magnification × 140); (b–d) line-field confocal optical coherence tomography in (b) vertical and (c, d) three-dimensional mode, and (e) dermoscopy (original magnification × 10). Note the hyporeflective ovoid structures/lobules of different sizes in the dermis (arrow), pushing towards the thinned epidermis and surrounded by stromal reaction (star).

For sBCCs, atypical keratinocytes were noticed in 81.1% of cases, while an altered DEJ profile, tumour nests/lobules, white hyper-reflective stroma and prominent vessels were seen in 100% of cases. Cell polarization was seen in 72.7% of cases, and the 'string of pearls' pattern in 90.9% (Figs 1 and 3, Figs S1 and S3).

By contrast, the infiltrative subtypes were characterized by the so-called 'shoal of fish' pattern (100%) (Fig. 4). Mixed subtypes equally displayed the 'string of pearls' patterns as well as deeper ovoid tumour nests/lobules with no connection to the epidermis.

Agreement

The overall BCC subtype agreement between LC-OCT and conventional histology was 90.4% (95% CI 79.0–96.8), compared with 84% for OCT and 62.5% for RCM.

The sensitivity, specificity, PPV and NPV values of LC-OCT for different BCC subtypes are shown in Table 2, with ROC curves in Fig. 5. Multinomial regression with stepwise selection of variables identified the following features as most useful in distinguishing BCC subtypes: epidermal thinning, atypical honeycomb pattern, prominent vessels/neoangiogenesis, shoal of fish pattern, string of pearls pattern and white hyper-reflective stroma. Bidirectional elimination excluded (*en face*) tumour nests and (*en face*) clefting (Tables S2 and S3).

Discussion

In vivo BCC morphology has been widely characterized using, among others, the techniques of RCM and OCT. Longo *et al.* developed an RCM algorithm for differentiating BCC subtypes, with the key criteria being cord-like structures for sBCCs, large tumour nests and clefting for nBCCs, and dark silhouettes and abundant bright compact collagen for iBCCs.[10] Conventional OCT has been used for the noninvasive characterization of BCCs,[2,26–28] and the specific features identified were hyporeflective ovoid structures originating from the stratum basale/DEJ,

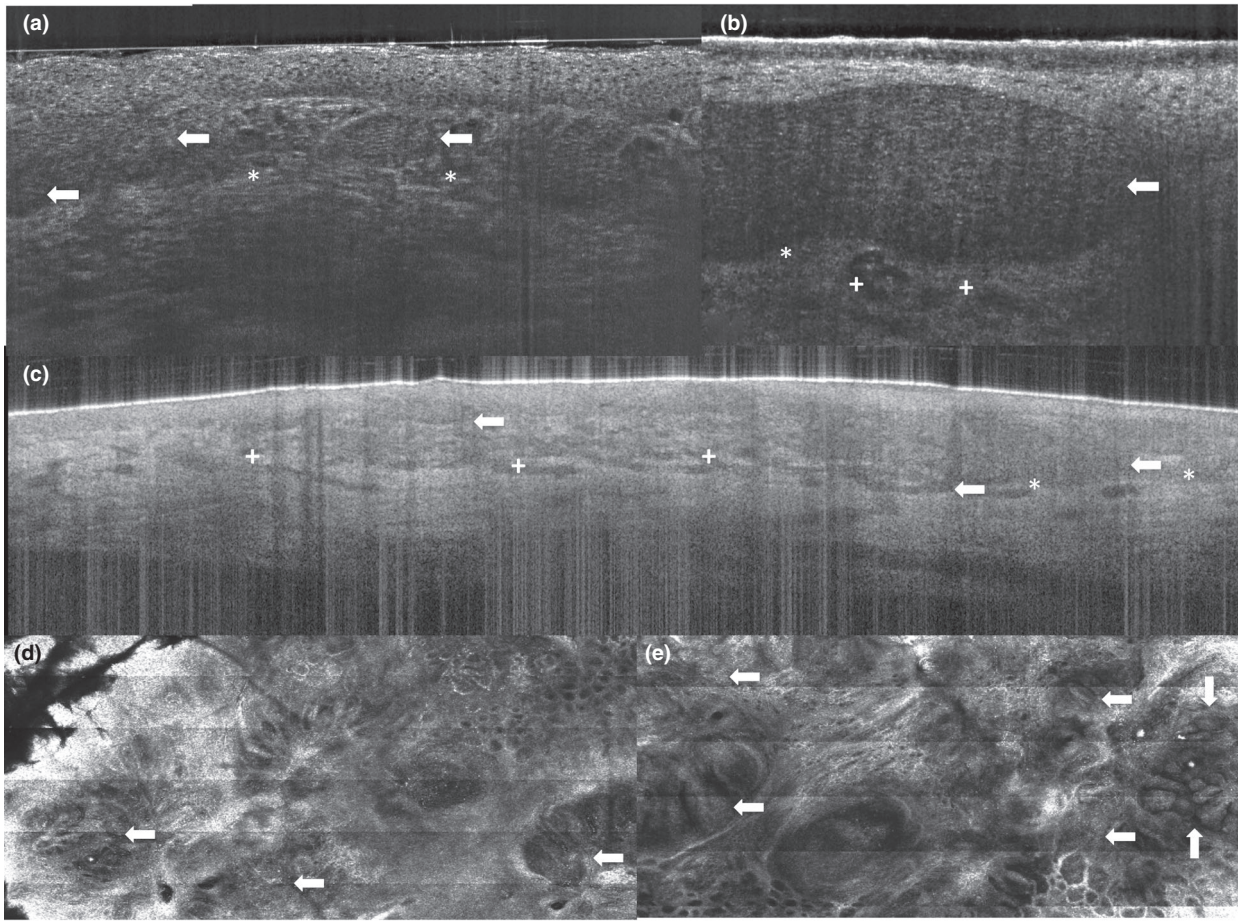

Figure 3 (a–e) Superficial basal cell carcinoma of the leg in a 54-year-old woman as visualized by (a, b) line-field confocal optical coherence tomography in vertical mode, (c) optical coherence tomography and (d,e) Vivastack reflectance confocal microscopy. Note the hyporeflective ovoid structures or tumour nests/lobules of different sizes in the dermis arranged in a string of pearls pattern (arrow), surrounded by stromal reaction (star) and dilated vessels (+).

corresponding to tumour nests, either with contact to the DEJ (string of pearls pattern) in sBCCs, or separated from the DEJ in nBCCs; and a dark rim, white hyper-reflective stroma, cysts and shoal of fish structures in iBCCs.[11] Dedicated Cochrane reviews have confirmed a role for both RCM and OCT in the diagnosis of clinically challenging BCCs.[9,12] In a pilot study, a combination of OCT and RCM showed good correlation to key histopathological features of infiltrative BCCs.[29]

LC-OCT can be seen as a method for combining the aforementioned diagnostic tools. LC-OCT images can be intuitively evaluated by physicians trained in non-invasive diagnostic technologies and with at least basic knowledge of skin histopathology. In fact, vertical (*en coupe*) scans are directly comparable to OCT images and histology, while horizontal (*en face*) scans can be related to RCM and dermoscopy. Preliminary studies conducted with available LC-OCT prototypes reported good correlations with histopathology in pilot settings.[14,30] However, there is a lack of systematic studies on large numbers of cases, with only one very recent study analysing 66 BCCs of pure histological subtypes.[18] Suppa *et al.* described lobules, blood vessels and small bright cells within epidermis as the most common criteria for BCCs. They also associated hemispheric lobules, connection with the epidermis and absence of stretching of the stroma with sBCCs; macrolobules, absence of connection to the epidermis with nBCCs; and branched lobules with iBCCs.[18] We observed similar features, but we have described our nomenclature based on the standard histological patterns, known RCM criteria for cytology and known OCT criteria for morphology.

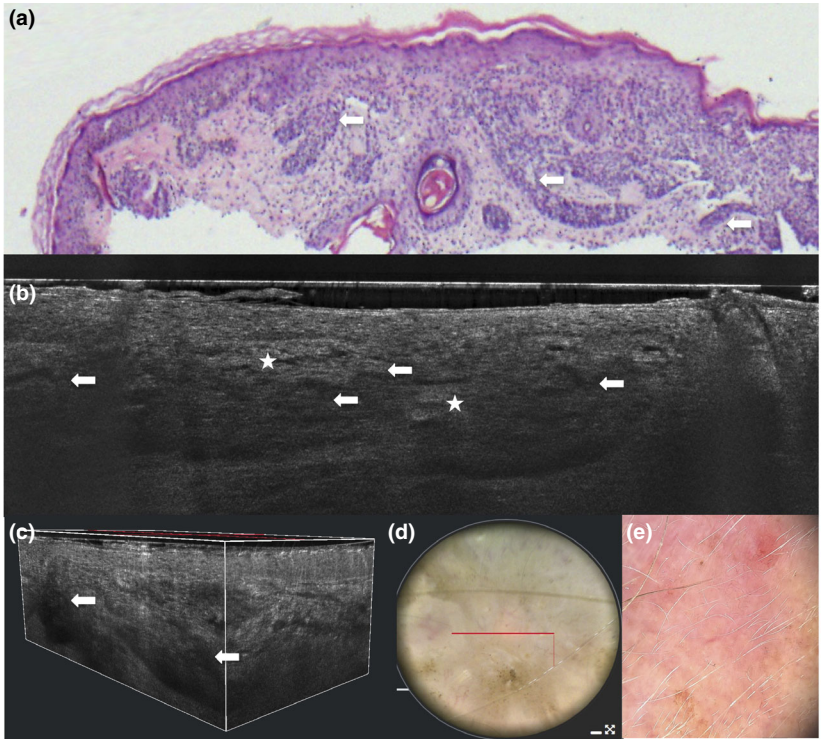

Figure 4 (a–e) Infiltrative basal cell carcinoma of the face in a 60-year-old man as visualized by (a) conventional microscopy (haematoxylin and eosin, original magnification × 40), (b, c) line-field confocal optical coherence tomography in (b) vertical and (c) three-dimensional mode, (d) clinical examination and (e) dermoscopy (original magnification × 10). Note the bizarrely configured, hyporeflective, branched strands arranged in a shoal of fish pattern (arrow), separated by a discrete stromal reaction (star).

The most intuitive BCC feature in our analysis is the tumour nest/lobule, which corresponds to its histological counterpart. Dark peritumoral clefting corresponding to mucin clearly delimitates the nests, which are surrounded by a bright collagenic stromal reaction in most cases.

Compared with conventional OCT, LC-OCT provides a higher resolution, which allows visualization of cellular components. In particular, larger cells, such as keratinocytes and activated melanocytes, can be clearly seen. In BCCs, slightly atypical keratinocytes in the epidermis and atypical cells in the tumour/lobules (described as cells of different sizes, shapes and contours) are visible. The cells in the tumour nests/lobules are hyporeflective with a hyper-reflective border and can either be polarized in overlapping strands or sometimes occur in a classic peripheral palisading. Analogously, pigmented BCCs sometimes show more hyperreflective components, possibly corresponding to melanocytes infiltrating the BCC, or to melanophages or pigmented keratinocytes, in line with previous experience with RCM and OCT.

The alteration of the DEJ seen in RCM and OCT becomes an alteration of the DEJ profile in LC-OCT compared with healthy skin, as tumour nests/lobules appear to be either connected to the epidermis (in sBCCs) or pushing it upwards (in nBCCs).

In our experience, nBCCs are extremely well characterized with ovoid nests/lobules in the dermis, pushing against the DEJ and causing a thinning of the epidermal layers. Micronodular tumours were also distinguishable by their smaller lobular components. Sometimes, dark holes were seen inside the nests, probably due to cysts and/or necrosis.

In the case of sBCCs, the tumour nests/lobules, which were slightly elongated, were clearly identifiable as a series of small ovoid nests/lobules connected with the DEJ and with each other through streamlined cords (string of pearls pattern). In contrast to conventional OCT, however, the epidermis does not appear irregularly thickened, but can be mostly distinguished from the tumour lobules connected to it.

Infiltrative tumours are usually more difficult to diagnose, as they do not have well-defined roundish

Table 2 Diagnostic accuracy of line-field confocal optical coherence tomography in detecting different basal cell carcinoma subtypes.

BCC type	Point estimates (95% CI)
Nodular	
Apparent prevalence	0.48 (0.34–0.62)
True prevalence	0.48 (0.34–0.62)
Sensitivity	0.96 (0.80–1.00)
Specificity	0.96 (0.81–1.00)
Positive predictive value	0.96 (0.80–1.00)
Negative predictive value	0.96 (0.81–1.00)
Positive likelihood ratio	25.92 (3.78–177.68)
Negative likelihood ratio	0.04 (0.01–0.28)
Kappa	0.92 (0.82–1.00)
AUC	0.96 (0.91–1.00)
Superficial	
Apparent prevalence	0.17 (0.08–0.30)
True prevalence	0.21 (0.11–0.35)
Sensitivity	0.82 (0.48–0.98)
Specificity	1.00 (0.91–1.00)
Positive predictive value	1.00 (0.66–1.00)
Negative predictive value	0.95 (0.84–0.99)
Positive likelihood ratio	Inf (NaN–Inf)
Negative likelihood ratio	0.18 (0.05–0.64)
Kappa	0.88 (0.71–1.00)
AUC	0.98 (0.95–1.00)
Infiltrative BCCs	
Apparent prevalence	0.12 (0.04–0.23)
True prevalence	0.10 (0.03–0.21)
Sensitivity	1.00 (0.48–1.00)
Specificity	0.98 (0.89–1.00)
Positive predictive value	0.83 (0.36–1.00)
Negative predictive value	1.00 (0.92–1.00)
Positive likelihood ratio	47.00 (6.76–326.73)
Negative likelihood ratio	0.00 (0.00–NaN)
Kappa	0.90 (0.70–1.00)
AUC	0.92 (0.75–1.00)
Nodular–superficial BCCs	
Apparent prevalence	0.23 (0.13–0.37)
True prevalence	0.21 (0.11–0.35)
Sensitivity	0.91 (0.59–1.00)
Specificity	0.95 (0.83–0.99)
Positive predictive value	0.83 (0.52–0.98)
Negative predictive value	0.97 (0.87–1.00)
Positive likelihood ratio	18.64 (4.76–72.94)
Negative likelihood ratio	0.10 (0.01–0.62)
Kappa	0.83 (0.65–1.00)
AUC	0.90 (0.79–1.00)

AUC, area under the curve; Inf, infimum; NaN, not a number (undefined).

nests but rather elongated, slightly hyporeflective strands/branched lobules, surrounded by a bright collagen reaction. This feature defines the 'shoal of fish' pattern, also visible in OCT.

BCC subtyping is crucial for choosing an appropriate therapy, while superficial and thin nodular BCCs can

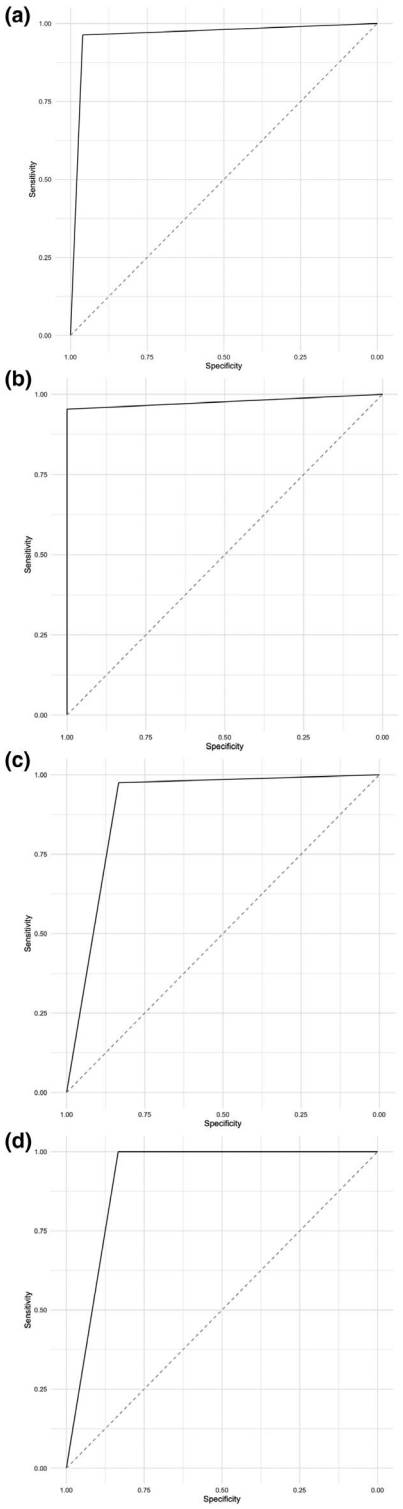

Figure 5 Receiver-operating characteristic curves: (a) nodular basal cell carcinoma (BCC), (b) superficial BCC, (c) infiltrative BCC and (d) nodular–superficial BCC.

be treated with local therapy options, thick nodular and infiltrative BCCs should be excised with (Mohs) surgery. Up to 40% of BCCs in daily clinical practice are of mixed subtype, and a normal punch biopsy is often too small to ensure complete lesion sampling.[31]

In vivo mapping with LC-OCT is able to scan the whole lesion and is able to identify the individual components of mixed tumours, providing an advantage compared with standard punch biopsies.

In our analysis, one case of superficial BCC was wrongly evaluated as nodular–superficial, probably due to numerous sebaceous glands acting as confounders; such entities appear as roundish hyporeflective structures with hyper-reflective borders, usually containing lobules of large (sebaceous) cells. To avoid confounding, we suggest combined evaluation of vertical and horizontal images, as sebaceous glands and sebaceous hyperplasia appear in horizontal mode as sharply demarcated, concentric, roundish structures in continuity with hair follicles, in contrast to BCC tumour nests.

In LC-OCT horizontal sections, the following BCC patterns were found: an atypical honeycomb pattern defined by polygonal bright keratinocytes of different sizes, shapes and contours; canalicular blood vessels; bright collagen stromal reaction/elastosis; and ovoid hyporeflective tumour nests with dark clefting and palisading. In our experience, these characteristics appeared less well defined than with RCM.

In our opinion, the main advantages of LC-OCT are the nearly cellular resolution and the good penetration depth reaching the dermis, combined with the instant switch from vertical to horizontal mode, the user-friendly software and the fast camera-guided image acquisition in three dimensions, which allows navigation of the whole tumour.

Nevertheless, some limitations exist. For example, distinguishing between nBCCs and sBCCs can sometimes be difficult, the tight connection of the tumour islands to the DEJ might be overlooked. In addition, some deep nodular components might not be visualized because of limits to the penetration depth of LC-OCT (which is less than conventional OCT), so that the possibility of missing deeper nodular components exists. For the same reason, determination of BCC thickness of the BCC is limited with LC-OCT compared with conventional OCT, as it is with RCM. Infiltrative BCCs require caution, as elongated tumour strands can sometimes be misinterpreted as blood vessels by nonexpert observers. Some significant differential diagnoses, for example with melanocytic tumours, are more difficult using LC-OCT compared with RCM because of the slightly lower resolution of the LC-OCT device. All the cited technologies can encounter limits in scanning difficult-to-reach anatomical areas, such as the inner eyelids. In doubtful cases, short-term follow-up or a biopsy should be performed.

This work was limited by the smaller number of iBCCs and RCM/OCT acquisitions. Moreover, the multiple but small Vivastacks images for mapping the whole tumour area might be responsible for the lower diagnostic confidence attributed to RCM. A larger, systematic comparison study should be conducted to further analyse the advantages and pitfalls of the different technologies.

Conclusion

Our study describes the most common LC-OCT features of BCCs compared with histological findings, and shows that the device provides significant additional morphological details compared with naked eye examination and dermoscopy for diagnosing BCCs and their histological subtypes. This could have important practical consequences as it allows the clinician to immediately assign the correct treatment for the patient. Similar to other, already established, noninvasive diagnostic methods, LC-OCT is quick, painless and intuitively comparable to histology following dedicated training.

Acknowledgement

We thank DAMAE Medical for providing the LC-OCT device used for this study.

What's already known about this topic?

- The novel imaging technique of LC-OCT has been shown in small case series to be able to noninvasively characterize healthy skin and potentially nonmelanoma skin cancer, as a result of its good resolution and penetration depth.
- There is to date just one systematic study defining the LC-OCT diagnostic criteria for BCC.

What does this study add?

- LC-OCT is useful for the *in vivo* diagnosis and characterization of BCC subtypes with high sensitivity and specificity compared with histology.
- The comparison with other imaging technologies shows the advantages and limitations of this new imaging method.

References

1 Peris K, Fargnoli MC, Garbe C *et al*. Diagnosis and treatment of basal cell carcinoma: European consensus-based interdisciplinary guidelines. *Eur J Cancer* 2019; **118**: 10–34.

2 Nori S, Rius-Díaz F, Cuevas J *et al*. Sensitivity and specificity of reflectance-mode confocal microscopy for in vivo diagnosis of basal cell carcinoma: a multicenter study. *J Am Acad Dermatol* 2004; **51**: 923–30.

3 Garbarino F, Migliorati S, Farnetani F *et al*. Nodular skin lesions: correlation of reflectance confocal microscopy and optical coherence tomography features. *J Eur Acad Dermatol Venereol* 2020; **34**: 101–11.

4 Manfredini M, Arginelli F, Dunsby C *et al*. High-resolution imaging of basal cell carcinoma: a comparison between multiphoton microscopy with fluorescence lifetime imaging and reflectance confocal microscopy. *Skin Res Technol* 2013; **19**: e433–43.

5 Paganelli A, Garbarino F, Ciardo S *et al*. Disguised basal cell carcinomas: how to track them down with reflectance confocal microscopy. *J Eur Acad Dermatol Venereol* 2020; **34**: e68–70.

6 Peccerillo F, Mandel V, Di Tullio F *et al*. Lesions mimicking melanoma at dermoscopy confirmed basal cell carcinoma: evaluation with reflectance confocal microscopy. *Dermatology* 2019; **235**: 35–44.

7 Ulrich M, Themstrup L, de Carvalho N *et al*. Dynamic optical coherence tomography in dermatology. *Dermatology* 2016; **232**: 298–311.

8 Boone M, Suppa M, Pellacani G *et al*. High-definition optical coherence tomography algorithm for discrimination of basal cell carcinoma from clinical BCC imitators and differentiation between common subtypes. *J Eur Acad Dermatol Venereol* 2015; **29**: 1771–80.

9 Dinnes J, Deeks JJ, Chuchu N *et al*. Reflectance confocal microscopy for diagnosing keratinocyte skin cancers in adults. *Cochrane Database Syst Rev* 2018; (12): CD013191.

10 Longo C, Lallas A, Kyrgidis A *et al*. Classifying distinct basal cell carcinoma subtype by means of dermatoscopy and reflectance confocal microscopy. *J Am Acad Dermatol* 2014; **71**: 716–24.e1.

11 Sinx KAE, van Loo E, Tonk EHJ *et al*. Optical coherence tomography for noninvasive diagnosis and subtyping of basal cell carcinoma: a prospective cohort study. *J Invest Dermatol* 2020; **140**: 1962–7.

12 Ferrante di Ruffano L, Dinnes J, Deeks JJ *et al*. Optical coherence tomography for diagnosing skin cancer in adults. *Cochrane Database Syst Rev* 2018; (12): CD013189.

13 Pedrazzani M, Breugnot J, Rouaud-Tinguely P *et al*. Comparison of line-field confocal optical coherence tomography images with histological sections: validation of a new method for in vivo and non-invasive quantification of superficial dermis thickness. *Skin Res Technol* 2020; **26**: 398–404.

14 Ruini C, Sattler E. Konfokale Line-Field-OCT: die eierlegende Wollmilchsau? [Line-field confocal optical coherence tomography: the golden goose?] (in German). *Aktuelle Dermatol*. 2020; **46**: 148–51.

15 Monnier J, Tognetti L, Miyamoto M *et al*. In vivo characterization of healthy human skin with a novel, non-invasive imaging technique: line-field confocal optical coherence tomography. *J Eur Acad Dermatol Venereol* 2020; **34**: 2914–21.

16 Ruini C, Schuh S, Pellacani G *et al*. In vivo imaging of *Sarcoptes scabiei* infestation using line-field confocal optical coherence tomography. *J Eur Acad Dermatol Venereol* 2020; **34**: e808–9.

17 Ruini C, Schuh S, Sattler E, Welzel J. Line-field confocal optical coherence tomography – practical applications in dermatology and comparison with established imaging methods. *Skin Res Technol* 2021; **27**: 340–52.

18 Suppa M, Fontaine M, Dejonckheere G *et al*. Line-field confocal optical coherence tomography of basal cell carcinoma: a descriptive study. *J Eur Acad Dermatol Venereol* 2020; **27**: 340–52.

19 Ogien J, Levecq O, Azimani H, Dubois A. Dual-mode line-field confocal optical coherence tomography for ultrahigh-resolution vertical and horizontal section imaging of human skin in vivo. *Biomed Opt Express* 2020; **11**: 1327.

20 Dubois A, Levecq O, Azimani H *et al*. Line-field confocal time-domain optical coherence tomography with dynamic focusing. *Opt Express* 2018; **26**: 33534–42.

21 Ogien J, Daures A, Cazalas M *et al*. Line-field confocal optical coherence tomography for three-dimensional skin imaging. *Front Optoelectron* 2020; **13**: 381–92.

22 Holmes J, von Braunmühl T, Berking C *et al*. Optical coherence tomography of basal cell carcinoma: influence of location, subtype, observer variability and image quality on diagnostic performance. *Br J Dermatol* 2018; **178**: 1102–10.

23 Themstrup L, De Carvalho N, Nielsen SM *et al*. In vivo differentiation of common basal cell carcinoma subtypes by microvascular and structural imaging using dynamic optical coherence tomography. *Exp Dermatol* 2018; **27**: 156–65.

24 De Carvalho N, Schuh S, Kindermann N *et al*. Optical coherence tomography for margin definition of basal cell carcinoma before micrographic surgery-recommendations regarding the marking and scanning technique. *Skin Res Technol* 2018; **24**: 145–51.

25 Welzel J, Schuh S. [Non-invasive diagnostics in dermatology] (in German). *J Dtsch Dermatol Ges* 2017; **15**: 999–1017.

26 Olsen J, Themstrup L, De Carvalho N *et al*. Diagnostic accuracy of optical coherence tomography in actinic keratosis and basal cell carcinoma. *Photodiagnosis Photodyn Ther* 2016; **16**: 44–9.

27 Ulrich M, Braunmuehl T, Kurzen H *et al*. The sensitivity and specificity of optical coherence tomography for the

assisted diagnosis of nonpigmented basal cell carcinoma: an observational study. *Br J Dermatol* 2015; **173**: 428–35.
28 Schuh S, Kaestle R, Sattler EC, Welzel J. Optical coherence tomography of actinic keratoses and basal cell carcinomas – differentiation by quantification of signal intensity and layer thickness. *J Eur Acad Dermatol Venereol* 2016; **30**: 1321–6.
29 Gill M, Sahu A, Alessi-Fox C *et al*. Angulated small nests and cords: key diagnostic histologic features of infiltrative basal cell carcinoma can be identified using integrated reflectance confocal microscopy-optical coherence tomography. *J Cutan Pathol* 2020; **48**: 53–65.
30 Dubois A, Levecq O, Azimani H *et al*. Line-field confocal optical coherence tomography for high-resolution noninvasive imaging of skin tumors. *J Biomed Opt* 2018; **23**: 1–9.
31 Cohen PR, Schulze KE, Nelson BR. Basal cell carcinoma with mixed histology: a possible pathogenesis for recurrent skin cancer. *Dermatol Surg* 2006; **32**: 542–51.

Supporting Information

Additional Supporting Information may be found in the online version of this article:

Figure S1. (a–d) Nodular basal cell carcinoma on the face of a 75-year-old woman as visualized under (a,b) line-field confocal optical coherence tomography in (a) vertical and (b) horizontal mode, (c) optical coherence tomography and (d) Vivastack reflectance confocal microscopy. Note the hyporeflective ovoid structures/lobules of different size in the dermis (arrow), surrounded by stromal reaction (*).

Figure S2. (a–d) Superficial basal cell carcinoma on the back of a 47-year-old man as visualized under (a) conventional microscopy (haematoxylin and eosin, original magnification × 100), (b) line-field confocal optical coherence tomography in vertical mode and (c) dermoscopy (original magnification × 10). Note the hyporeflective ovoid structures arranged in a string of pearls pattern (arrow), surrounded by a dark rim corresponding to peripheral clefting (*).

Figure S3. (a–c) Superficial basal cell carcinoma of the leg in a 54-year-old woman as visualized under (a) conventional microscopy (haematoxylin and eosin, original magnification × 100), (b) line-field confocal optical coherence tomography in vertical mode and (c) dermoscopy (original magnification × 10). Note the hyporeflective ovoid structures arranged in a string of pearls pattern (arrow), surrounded by dark rims corresponding to peripheral clefting (*). A hyperkeratotic crust (triangle) overlies the epidermal layer. Additionally, a sebaceous gland (rhombus) is visible.

Table S1. Main dermoscopy features of BCCs evaluated in the study with their relative and absolute frequencies.

Table S2. Multinomial logistic regression with stepwise selection of variables to search for LCOCT characteristics helping in the distinction of BCC subtypes.

Table S3. Final model.

Video S1. Line-field confocal optical coherence tomography three-dimensional acquisition of a pigmented nodular basal cell carcinoma.